Jurnal MIPA dan Pembelajarannya
e-issn: 2798-0634, email: jmipap.journal@um.ac.id

VOL	ISS	YEAR	DOI
6	4	2026	10.17977/um067.v6.i4.2026.2

SIMULATION STUDY OF HIGH-PERFORMANCE THIN FILM SOLAR CELL BASED OF PEROVSKITE N- CDS/P- $CH_3NH_3SnI_3$

Raed M. Humaidan[a*], Naziha N. Aneizan[a**], Ghaith Thaaer Fadhil Al-Doori[b***]

[a]General Directorate of Education Salahaddin, Ministry of Education, Salahaddin, Iraq
[b]Al-Dour Technical Institute, Northern Technical University, Iraq
Corresponding author, email: ramahr1980@gmail.com*, nazehanassar5@gmail.com**, ghaith.tf@ntu.edu.iq***

Keywords
Perovskite Solar Cell
PC1D Software
CH3NH3SnI3
Thin Films

Abstract
Solar cells fabricated of perovskite metal halide have experienced major improvement in the last few years. There is research interest in lead-free perovskite solar cells (PSCs) because lead in lead halide perovskites is believed to be toxic. CH3NH3SnI3 seems to be a good alternative to CH3NH3PbX3. The impact of different parameters on the performance of the perovskite solar cells was learned by us in this paper through the software PC1D simulation. The cell configuration is made of three layers of n- CdS/p- CH3NH3SnI3/p- InP. In this study, I explore the effect of varying CH3NH3SnI3 absorber layer thickness and doping concentration 0.5 to 5 µm and 1015 to 10 -3 without a back surface field (BSF) layer. The n-CdS/p-CH3NH3SnI3 heterojunction was enhanced with a BSF layer to enhance solar cell performance. The effect of the thickness and doping concentration of the Back Surface Field layer (of 0.5 _ 5) µm and 1015 -1020 cm-3 respectively were explored. The optimal doping concentration and thickness of the p- CH3NH3SnI3 and p-InP layers yielded the highest efficiency η = 24. 78 A/cm2 Jsc 34mA/cm2, Voc=0.81 and FF=90 A. The cell operating temperature was also experimented and the range was deposited between 300k to 400k and the findings revealed that the optimum was at 300k.

1. Introduction

Our world is losing its energy sources very rapidly. Solar energy is becoming another source of energy besides wind, biomass, and geothermal energy. Solar energy is the most plentiful of sources of energy and it is the most environmentally friendly, which presents a practical solution to current growing concerns regarding global warming and greenhouse gas emissions due to fossil energy use. The last four decades are marked with tremendous improvements in the cost-effectiveness and efficiency of silicon solar cells (Green et al., 2012; Hamoodi et al., 2022). They are supplying grid-based electricity at the prices that are affordable to fossil fuels in some parts of the world. New technologies in the technology portfolio include semiconductor-based technologies through thin-film deposition, including organic/inorganic and inorganic semiconductors only (Britt & Ferekides, 1993; Repins et al., 2008). In the last ten years, there have been major research studies that have unveiled second and third-generation solar cells that are currently known to be easy to make, cost-effective to produce and have superior efficiency. Therefore, such solar cells are highly available, mass-produced and applied to buildings in their low power applications. Nonetheless, in order to gain wider acceptance in the market, the price per watt ought to be decreased to the level of fossil fuel generated energy.

Remarkably, a new promising alternative in the field has risen with organometallic halide Perovskites (Green et al., 2014). Perovskites are free of lead and this has attracted tremendous research interest due to their stability and safety. Compounds such as $CH_3NH_3SnI_3$ can be used as a replacement to solar cells which are environmentally friendly. The best method to substitute Pb is to use elements that belong to the same group e.g. Sn and Ge. A mixture of monovalent and trivalent cations, whose overall structure is A2BIBIIIX6, with BI possibly Li and Na and K and Rb and Cs and

Ag and BIII possibly Al or Ga or In or Sb or Bi, could also be a replacement of Pb. Among them, Cs2AgBiX6 and Cs2(Ag/Na/K) (Bi/In)X6 are highly stable, and they are well-investigated in the recent past. Among all of these properties, the most promising one is Sn-based perovskite materials. (López-Ernández et al., 2024). $CH_3NH_3SnI_3$ has the property of increased hole mobility, and increased electron mobility, and these are essential in the charge transport (Nahid et al., 2024).

$CH_3NH_3PbI_3$ is popular as an active material in the solar cells, however, its lead content causes environmental and health hazards and its functionality is impaired by exposure to water, making it unstable (Li et al., 2016; Qin et al., 2014). Researchers are, therefore, looking at plausible alternatives. Tin perovskite solar cells have been demonstrated to be promising owing to their stability, a wider range of coverage by the visible spectrum, and limited recombination. Reduced diffusion length of Sn-based cells enhances the generation of electrons around the electron collector layer, improves electron collection and minimizes recombination (Noel et al., 2014; Song et al., 2017). $CH_3NH_3SnI_3$, a high-absorption coefficient material with a low bandgap (around 1.3 eV), has been demonstrated to operate with power conversion efficiencies greater than 20% (Du et al., 2016). Nonetheless, it has a bad morphology and is prone to moisture, oxygen, and heat which are major limitations (Singh et al., 2019). Besides optimizing the absorber material, transport layers is important in the determination of the PSC efficiency and stability. The electron transport layer (ETL) and hole transport layer (HTL) enable the extraction of charge and inhibits the undesirable recombination. Different ETL materials, such as TiO_2, ZnO, CdS, and CeO_2 are examined to increase the electron mobility and stability of the device.

CdS is a II-VI group semiconductor with a bandgap 2.45 eV. The CdS thin film has aroused the interest of researchers over a long duration of time because of its intriguing optoelectronic characteristics. It is an opaque coating that is commonly applied to the top of solar cells due to its excellent optoelectronics nature. Thickness variation is easily controlled to produce optical transparency of the film (Kapadnis et al., 2020).

InP is a III-V semiconductor that has a direct band gap of 1.35 eV. InP has a greater electron saturation velocity and electron mobility than silicon, and is noisier in devices. Also InP has been reported as a super-radio resistance material indicating the prospective application of InP based solar cells in space power systems (Ram Sevak et al., 2023).

2. Method

2.1. Simulation for PC1D Software

It is a computer program written to run on a personal computer compatible with the IBM product to solve fully coupled nonlinear equations of electron behaviour and of hole transport in quasi one-dimensional flake of semiconductor devices. Since it especially enables the simulation and analysis of the electrical and optical dynamics of photovoltaic devices it is highly convenient to enable researchers to gain insights. The first version of the program had been developed by Paul Basore and others at Sandia National Laboratories. It had additional developments by Dr. Don Clugston at the University of New South Wales, Australia, to increase its capabilities and turn it into a well-known instrument of solar cell studies and semiconductor apparatus modelling (Banerjee, 2015). The numerical methodology of PC1D is the two carrier semiclassical semiconductor transport equations. The assumptions made are as follows: The carrier carrier scattering (the two carriers flow independently), the hot carriers (the stray in carrier populations maintain thermal equilibrium with crystal lattice) and the carrier mobilities are isotropic, the energy levels offered to the electrons injected by the excitation do not cause a large change in the structure (rigid bands). It is assumed that the temperature of the device is constant, also, and that magnetic fields are removed. Electron and hole current density formulae are given (Jn, Jp) as functions of n, p, mu n, mu p and EFn, EFp).

$$J_n = \mu_n . n . \nabla E_{fn} \quad (1)$$

$$J_p = \mu_p . n . \nabla E_{fp} \quad (2)$$

The quasi-Fermi energies relative to their respective energy bands Determine which energy levels contain carriers of each type otherwise locally defined occupation of carriers. It is possible to apply a Boltzmann exponential approximation of the Fermi distribution function to non-degenerate materials.

$$n = N_c \cdot e^{-\frac{(E_c - E_{fn})}{K_B.T}} \quad (3)$$

$$p = N_V \cdot e^{-\frac{(E_{Ep} - E_V)}{K_B.T}} \quad (4)$$

By so doing they have employed Nc and Nv as effective density of states in conduction and valence band. Ec is the energy level at the conduction band edge and Ev is the level of energy at the valence band edge. By contrast degenerate doping effects must be added in such a way that the Ec and Ev can be perturbed in a manner that incorporates Boltzmann like effects. Nevertheless, despite the fact that this approach excludes degeneracy due to injection level excessively high, the influence of degeneracy should be taken into account. We lastly spend on the quasi-Fermi levels and the equilibrium Fermi energy levels at a chosen reference location to be analyzed separately (Pourdadash et al., 2014). fn and fp are the quasi-fermi potentials known as the quasi-Fermi Energy levels. With the PC1D framework, the reference is the using location of x=0. So, as to the point of view of the electrostatic potential and the spatial dependence of the bandstructure, we can carry out the concrete determination of the localization of conduction and valence band edges by applying Equations (3) and (4). The change of the band structure is determined by the introduction of band edge potentials V_n and V_p. They are potentials that relate to the conduction and valance band edge energy shifts by the electrostatic effect at a reference point. These changes in the majority of them are predominated mainly by the spatial variations of material composition or by the effect of narrowing band gaps due to the heavy doping. To be more precise, they affect the doping DEg Nc Nv band gap adjustment (DEgv).

$$V_n = \left(\frac{KT}{q}\right) ln\left(\frac{N_c}{N_{cr}}\right) + \frac{X - X_R}{q} + \Delta E_{gc} \quad (5)$$

$$V_p = \left(\frac{KT}{q}\right) ln\left(\frac{N_v}{N_{vr}}\right) - \frac{X - X_R}{q} + \Delta E_{gv} \quad (6)$$

q "represents the level of the elementary electronic charge. This reference point can be chosen such that the zero of the electrostatic potential lies conveniently at the location of the material properties (conduction and valence band) but not necessarily the reference point of the actual metal surface onto which the device is physically mounted. Here, we can define the electrostatic potential to have a zero in the neutral intrinsic situations. The introduction of these concepts leads to new pairs of Boltzmann-like expressions of n and p by the use of the equations (3,4).

$$n = n_{ir} e^{q(\Psi + V_n - \Phi_n)/KT} \quad (7)$$

$$p = n_{ir} e^{q(-\Psi + V_p + \Phi_p)/KT} \quad (8)$$

Here, nir is the concentration of carrier at the reference site.

On the behavior of all the electrons and all the holes défaisants entering the same volume, two other equations may be derived. Take-over into the volume, carrier formation within the volume (generation), The continuity equations can allow the recombination of the carriers within the volume.

$$\frac{\partial n}{\partial t} = \frac{\nabla . J_n}{q} + G_L - U_n \quad (9)$$

$$\frac{\partial p}{\partial t} = \frac{\nabla . J_p}{q} + G_L - U_p \quad (10)$$

GL is the rate of generation of electron of the photogeneration volume. Absorption Light pairs are handled, and Un and Up are the net volume electronic and hole recombination rates. We begin with a point to derive an equation of the charge density and the voltage of the electrons (electrostatic voltage Ψ) or the so called the Poisson's equation here to find a specific solution to the changes of the static fields within the semiconductors (Banerjee, 2015) and can be expressed as:

$$\nabla^2 \Psi = -\frac{\rho}{\epsilon} \quad (11)$$

In which ρ ρ is the volume charge density, and ϵ is the permittivity.

The equation below can be used to determine the current passing through the solar cell:

$$I = I_0 \left(exp \frac{eV}{K_B T} - 1 \right) \quad (12)$$

with I being the current in the load circuit, I0 is the saturation reverse current, T is the temperature and KB is the Boltzmann constant. Voltage of an open circuit (V_{oc}) can be determined by the following equation:

$$V_{oc} = \frac{K_B T}{e} ln \frac{I_{sc}}{I_o} + 1 \quad (13)$$

The most common parameter to define the I-V curve is the Square of the I-V curve the Fill Factor (FF) which in most situations is the solar cell resistance losses. This may be calculated using the following relation:

$$FF = \frac{P_{max}}{I_{sc} \times V_{oc}} = \frac{V_m \times I_m}{I_{sc} \times V_{oc}} \quad (14)$$

The conversion efficiency of the solar cell can be expressed as shown below:

$$\eta = \frac{FF \times V_{oc} \times I_{sc}}{P_{in}} \quad (15)$$

2.2. Device Structure and Simulation

Figure 1 shows the layout of the proposed $CH_3NH_3SnI_3$ solar cell. The design utilizes p type $CH_3NH_3SnI_3$ is the (peroviskite) absorber layer and the window layer is n type CdS. With the bandgap of the window layer sufficiently small, absorptive material with a large bandgap on the surface and low-bandgap absorptive material in the absorber layer is feasible, with the absorber layer being effectively absorptive to short wavelength photons in the solar spectrum: a practical implementation of this arrangement is possible. With the objective of assessing performance attributes of proposed solar cell, electrical characteristics of the cell have been studied in a systematic manner through PC1D simulation tool. The main parameters to be incorporated include the area of the gadget, the depth of the layer and the densities of the carrier, band gap, dielectric constant, bulk recombination as well as reflectance among others; this simulation program has been used to explain the electrical properties of the solar cell. The PC1D simulation is employed in this work; it is divided into two sections (i) design n-CdS/p- $CH_3NH_3SnI_3$ heterojunction solar cell without back surface field layer and (ii) the thickness absorber layer influence on the design was studied with the range values between 0.5 and 5 µm. The effect of the back ground doping of the $CH_3NH_3SnI_3$ absorber layer with the different values of (10^{15}-10^{20}) cm^{-3} and the second part of this paper was the introduction of the back surface field (BSF) to the n-CdS/p- CH3NH3SnI3 solar cell.

Performance studies of solar cells as a variable of thickness and concentration of doping of this layer were conducted in the following ranges; (0.5-5) µm and (10^{15}-10^{20}) cm^{-3} respectively. Table 1 gives the summary of the input settings of this program. All simulations were conducted at a constant temperature of 25 °C, and constant light intensity of 100 mW/cm^2 (AM)1.5G.

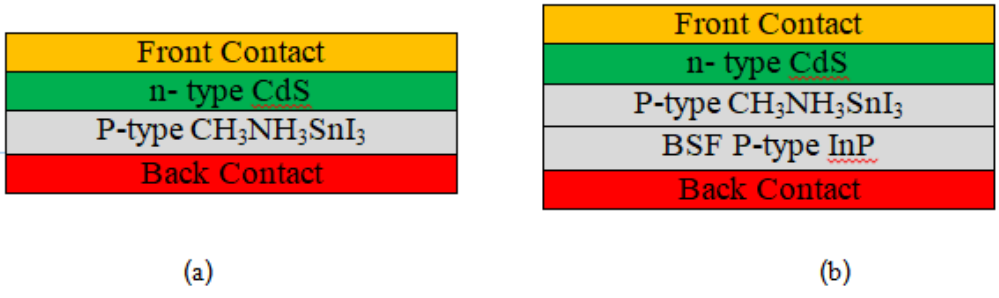

Figure 1 peroviskite solar cell (1) without and (2) with BSF layer (a) device structure and (b) energy payoff.

Table1. Parameters of materials inset in PC1D simulation tool.

Parameters	n- CdS	p- $CH_3NH_3SnI_3$	p- InP
Thickness (µm)	0.03	0.5-5	0.5-5
Dielectric constant(eV)	10	10	12.1
Energy Band Gap (eV)	2.45	1.3	1.35
Electron Affinity(eV)	4.4	4.2	4.4
Nc/Nv Ratio	0.12	1	0.042
Back ground doping (cm^{-3})	$1.18 \times 10^{17} cm^{-3}$	(10^{15}-10^{20}) cm^{-3}	(10^{15}-10^{20}) cm^{-3}
Electron mobility ($cm^2/V.s$)	350	1.6	4730
Hole mobility ($cm^2/V.s$)	50	1.6	151.5
Excitation mode	Transient	Transient	Transient
Temperature	K)300-400(	K)300-400(	K)300-400(
Constant intensity	$100mW/cm^2$	$100mW/cm^2$	$100mW/cm^2$
Primary light source	AM 1.5G Spectrum	AM 1.5G Spectrum	AM 1.5G Spectrum
Other parameters	Internal PC1D	Internal PC1D	Internal PC1D

3. Result and Discusion

The capacity of the solar cell to absorb solar radiation effectively depends on the thickness of the (perovskite) layer. In order to maximize the photocurrent, the thickness of the active layer should be thick enough to absorb light over a spectrum of wavelengths. Figure 2 shows that the absorption thickness of perovskite between 0.5 µm and 5 µm has an influence on the J-V characteristics. We discovered that as the (perovskite) Absorber Layer thickness increased the curve of I-V also increased due to the increased energy absorption and consequently the rate of the pair generation increases (electron - hole) to a point (Ngoupo et al., 2019).

Such a visualization of the short circuit current (J_{sc}), the open circuit voltage (V_{oc}), and the fill factor (FF%) is complete and is offered in Figure 3. Based on these parameters it is possible to determine the efficiency of the solar cell (η%. We observed that short circuit current increases with (9.4-25.3)mA/cm^2 and open circuit voltage as (0.83-0.81)Volt, it reduced slightly. Conversion efficiency (η) was found to increase from (7-18.2) with the increase in (peroviskite) absorber layer increasing (0.5-5) µm as indicated in the Figure 4.

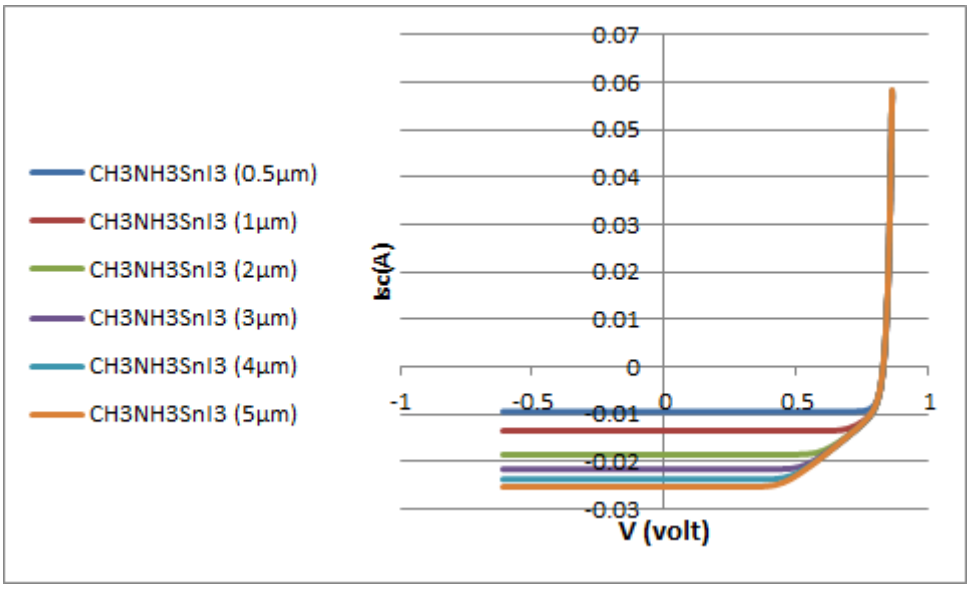

Figure 2. Influences of peroviskite thickness on the properties curve (I-V).

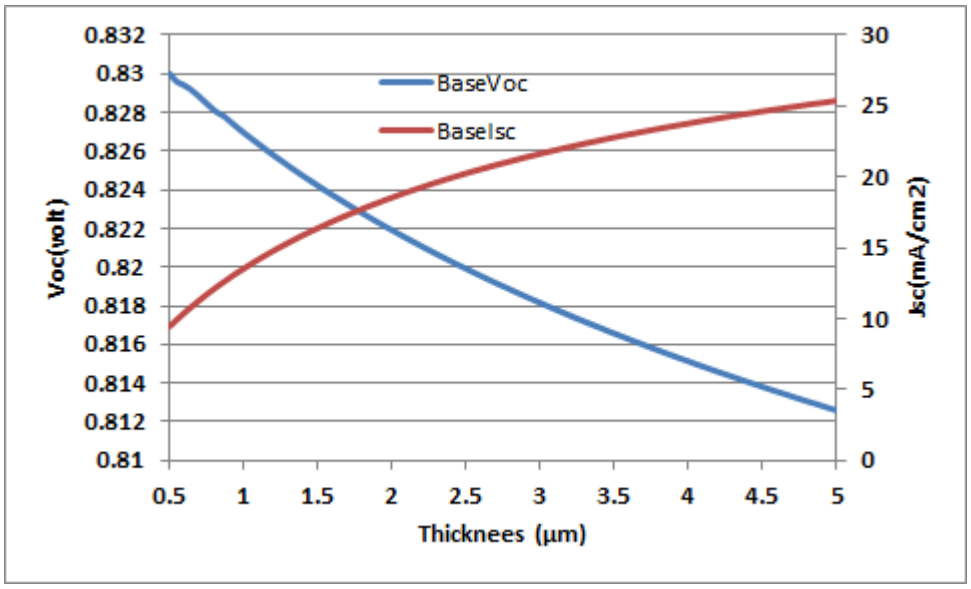

Figure 3. Dependence of short circuit current and open circuit voltage on peroviskite thickness (0.5-5) µm.

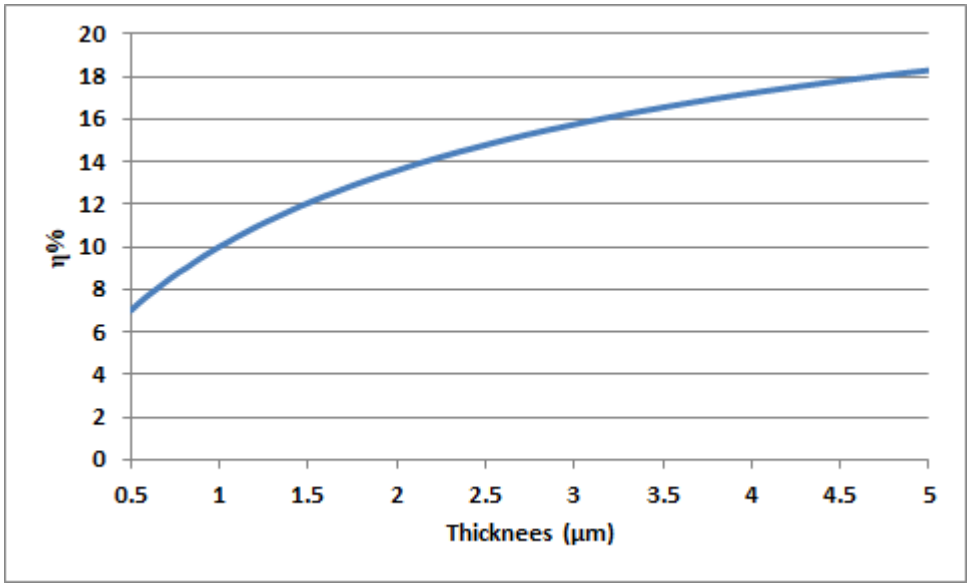

Figure 4. Variation conversion efficiency as a function of peroviskite thickness from (0.5-5)µm.

Doping is an extremely significant process that is employed to enhance the characteristics of semiconductor devices including solar cells. The electrical behavior of the layers, which determine the device performance, is determined by doping of a photoactive material in the solar cell architecture (Tuo et al., 2024). As shown in Figures 5, the baseline model was operated under the following conditions: 10^{15} cm^{-3} and 10^{20} cm^{-3} were the doping concentration of the (perovskite) absorber region.

Short circuit current density is constant of the doping concentration between 1×10^{15} cm^{-3} up to the point of 4.8×10^{18} cm^{-3}, where short circuit current value becomes lower as the doping concentration increases. The open circuit voltage slightly reduces as 0.80 V to 0.62 V with further increase in the doping concentration. The optimal efficiency is obviously 18.29 per cent. Efficiency declines drastically after the doping density of 1.18×10^{17} cm^{-3}, as illustrated in Figure 5, and hence in optimal range. This may be explained by the recombination mechanism at the rear contact of the solar cell. The technical explanation of this problem is that as the doping density in the absorber layer

increases, the depletion width decreases, the effective length increases making carrier collection difficult (Parajuli et al., 2022).

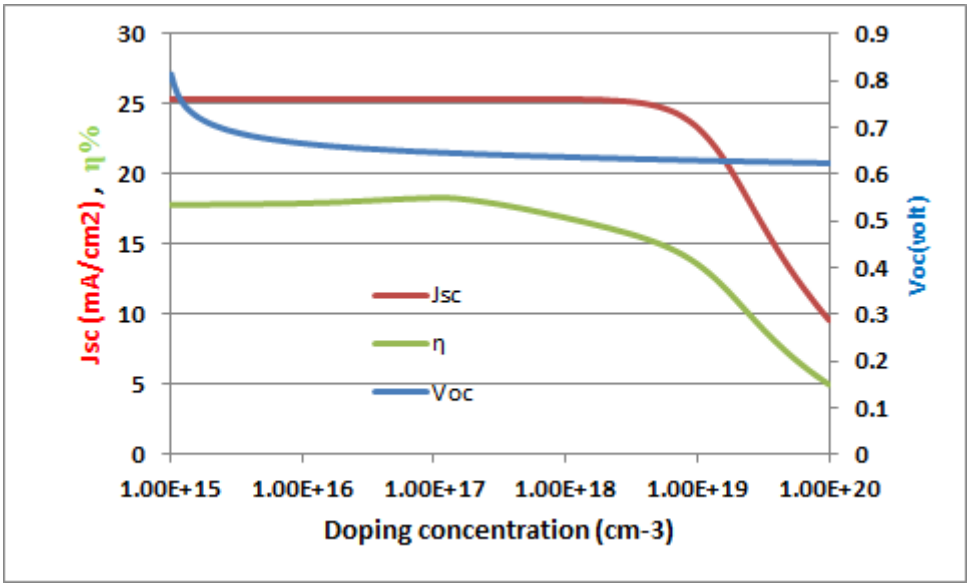

Figure 5. Plot of a short circuit current, open circuit voltage and conversion efficiency versus peroviskite layer doping concentration.

4.2 Effect of the Perovskite Layer Thickness on the Quantum Efficiency

A more precise definition would be Quantum Efficiency (QE), which is the ratio of quantity of charge carriers (electron-hole pairs) N el captured by a solar cell / quantity of incoming photons N ph of a given energy incident on a solar cell. It may be the function of energy, and even there the function of wavelength may be still further expressed, the case being, it is expressed by the following mathematical relationship (Luque & Hegedus, 2011).

$$EQE = \frac{N_{el}}{N_{ph}} = \frac{h.c.J_{sc}(\lambda)}{q\lambda.I_0(\lambda)} \quad (1)$$

H is the Planck constant, q the charge of an electron, c the speed of light, Jsc the short circuit current, l the wavelength of the exciter light and I0(l) electric current due to the photoelectric effect. In a case where quantum efficiency = the number of electrons produced/ the number of photons absorbed, then quantum efficiency of an ideal diode is 1. The incident light is however, part of which is reflected naturally, on the surface of the semiconductor, and the remainder of which is not absorbed in the depletion region. In this way the value of efficiency can be maximized by covering its surface with a non-reflective material. Among the important visual parameters in the solar cell applications is Quantum Efficiency (QE), which identifies the spread length, permanence of the minority carriers and the rate at which the surface is recombined by the front and the back surfaces. The quantum efficiency is 1 or 100 percent when all photons that the absorber layer absorbs and all the carriers created in it are collected (Duenow et al., 2007). The functions of Quantitative Efficiency (QE) are that of depletion region (W), diffusion length of minority charge carrier, absorption coefficient and wavelength respectively (Rassol et al., 2021). Figure 6 shows the thickness of the perovskite absorption layer ($CH_3NH_3SnI_3$) versus (0.5–5) µm and the Quantum Efficiency. It is noted that, at short wavelength, the Quantitative Efficiency is large and then it rapidly decreases with wavelength because of low absorption coefficient and makes the carrier generation rate to decrease and the recombination rate at the rear cell surface to also increase. On the other hand, Figure 6 suggests that quantum efficiency rises as absorber region thickness increases to imply that the falling photons of different wavelengths were captured at different cell depth. Thus, two-pair (electron-hole) generation will stabilize to a certain extent with the increase of absorber layer thickness.

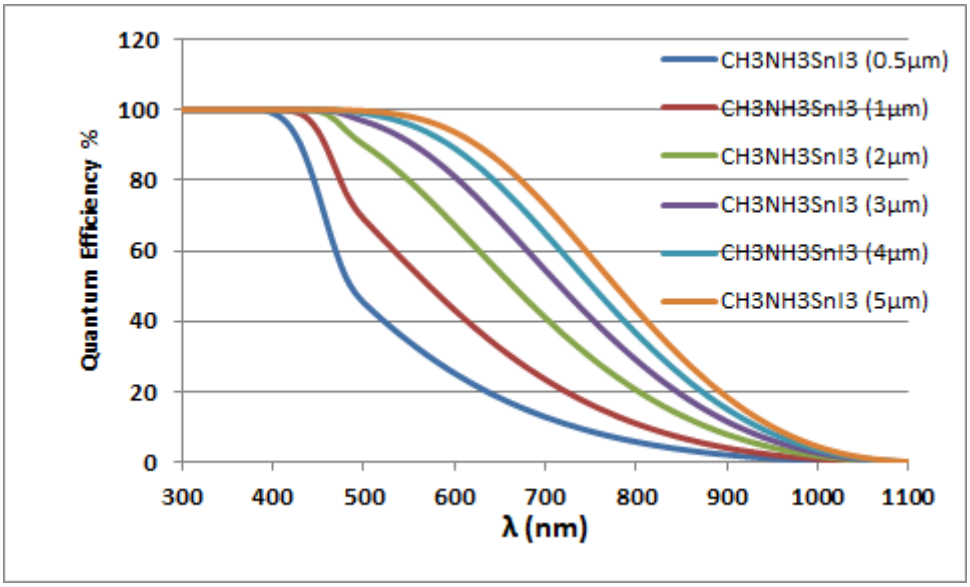

Figure 6. Effects of layer thickness of $CH_3NH_3SnI_3$ layer on Quantum Efficiency.

3.1. Impact of the Thickness of Back Surface Field Layer

The solar cell with the back surface field has a better spectral response than that of the solar cell without a back surface field (Lee et al., 2016). The BSF amend significantly the summation of carriers with long wavelengths of the solar spectrum by decreasing recombination at the backside of the BSF solar cell. Hence, the short-circuit current density rises. The open-circuit voltage is also improved because short-circuit current density rise and the supplemented potential energy between p-$CH_3NH_3SnI_3$ and p-InP layers (Ahmed et al., 2020). The BSF layer thickness is one of the key challenges in fabricating these solar cells as the BSF layer thickness must be ultrathin to maximize performance. InP was analyzed based on its photovoltaic (PV) properties, such as short circuit current density (Jsc), open circuit voltage (Voc), efficiency (η) and fill factor (FF) for a BSF layer thickness from 0.5 to 5 µm. Figure

7 illustrates Jsc increased from 31.5 mA/cm^2 to 34 mA/cm^2 and Voc increased a little from 0.817 V to 0.818 V when the BSF thickness was increased from 0.5 µm to 5 µm. As shown in Figure 8, the optimal BSF thickness is difficult to determine as the overall efficiency of the solar cell increased from 22.88% to 24.78% with increasing the BSF layer thickness. Nevertheless, for a high performance and practical solar cell, achievable and optimized p-InP BSF layer thickness must be well chosen to balance efficiency, stability and manufacturability.

The solar cell with and without a back surface field has a superior spectral response than the other (Lee et al., 2016). The BSF amend dramatically reduce the summation of the long wavelengths of the solar spectrum carriers by reducing recombination at the rear of the BSF solar cell. Therefore, current density on short-circuit increases. The open-circuit voltage is also enhanced since short-circuit current density increase and the supplemented potential energy between p-$CH_3NH_3SnI_3$ and p-InP layers (Ahmed et al., 2020). One of the major hurdles in the fabrication process of these solar cells is the BSF layer thickness because the thinnest BSF layer thickness must be used to maximize performance. InP was examined in terms of photovoltaic (PV) characteristics, including short circuit current density (Jsc), open circuit voltage (Voc), efficiency (η) and fill factor (FF) at a layer thickness of BSF of 0.5–5 mm. Figure 7 shows that Jsc increased by an increment of 31.5 mA/cm^2 to 34 mA/cm^2 and Voc increased slightly from 0.817 V to 0.818 V as BSF thickness was augmented from 0.5 to 5 µm. Figure 8 demonstrates that the optimal BSF thickness is hard to be established since the overall efficiency of the solar cell progressed to 24.78% instead of 22.88% with growing the BSF layer thickness. However, in order to have a high performance and feasible solar cell, an optimized p-InP BSF layer thickness should be selected appropriately to trade off efficiency, stability and manufacturability.

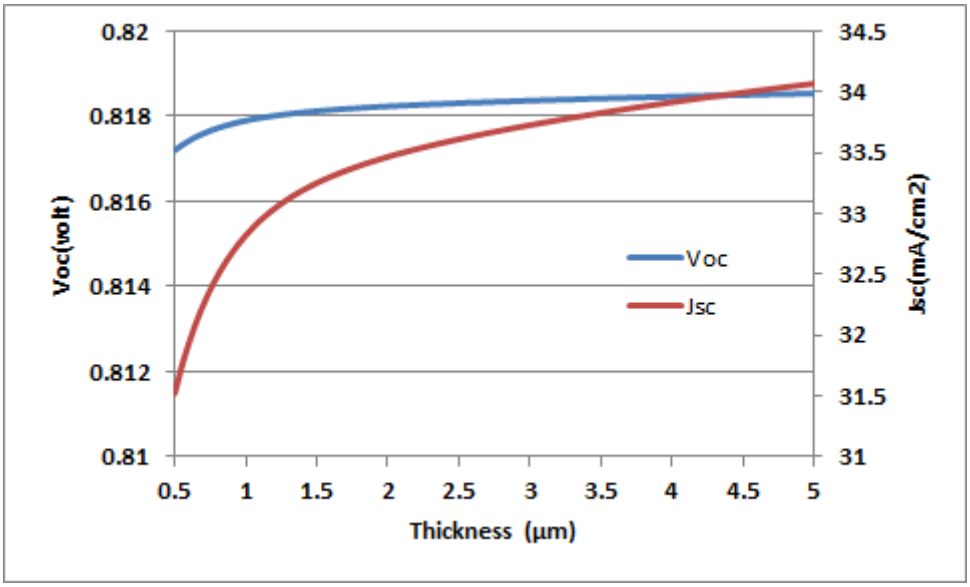

Figure 6. Variation of short circuit current and open circuit voltage as a function of BSF thickness from (0.5-5)µm.

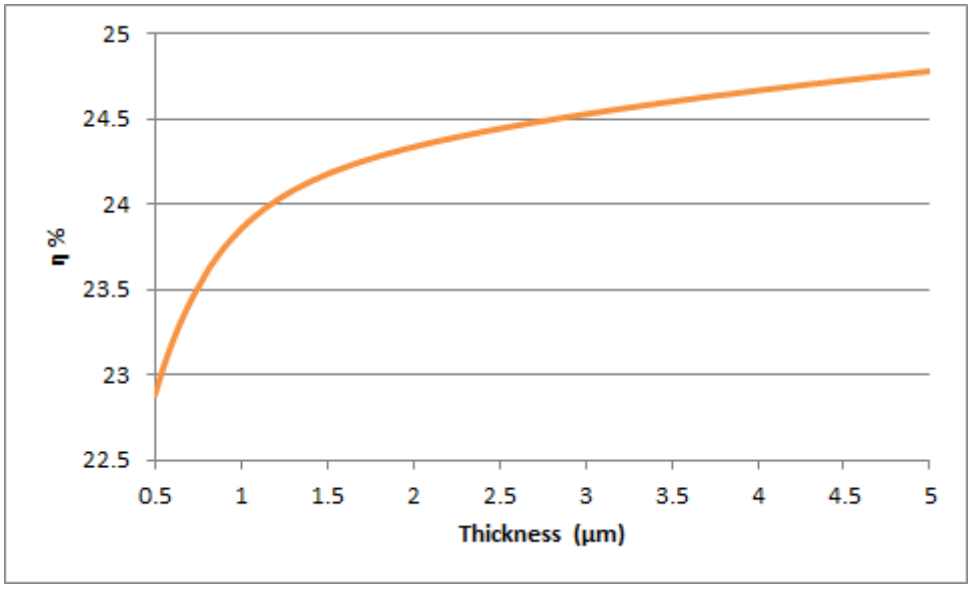

Figure 8. Variation conversion efficiency as a function of BSF thickness from (0.5-5)µm.

3.2. Impact of Doping Concentration in Back Surface Field Layer

Back surface field (BSF) is a significant component of a contemporary solar cell that is composed of heavily doped layer at the back of the solar cell. Electric field will be induced to the junction of low and highly doped region that poses as a barrier to the minority mobile charge carriers and minimize recombination within the rear layers of the solar cell (Mandong & Uzum, 2019). InP back surface layer solar cell was defined in the back surface layer doping concentration range (1×10^{15} cm^{-3} to 1×10^{20} cm^{-3}) and the photovoltaic properties (Jsc, Voc and η) were defined. Figure 9 demonstrates that doping concentration 4.8×10^{19} cm^{-3} has been used and the values of Jsc = 34 mA/cm^2, Voc = 0.81 V and η = 24.78% have been attained at 1.18×10^{17} cm^{-3} of doping concentration. Through the optimization, the optimal doping concentration of this optimized concentration is 1.18×10^{17} cm^{-3} in the back surface of the $CH_3NH_3SnI_3$ solar cell.

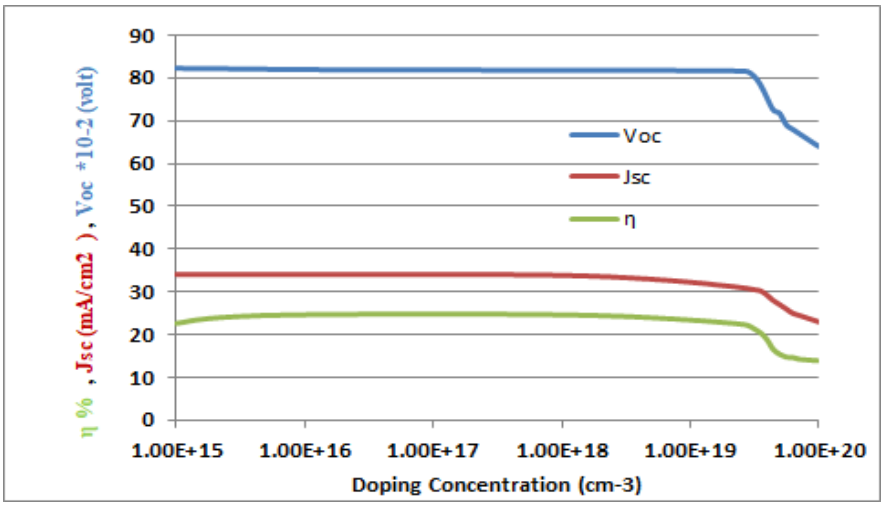

Figure 9. Jsc, Voc and eta were analyzed using a galvanic doping concentration of back surface field layer.

Following the theoretical simulation with pc1d software, the ultimate values of the n- CdS layer thickness were (0.03µm), the p- $CH_3NH_3SnI_3$ layer thickness was (5µm). The doping level of the n- CdS (1.18×10^{17} cm $^{-1}$) and p- $CH_3NH_3SnI_3$ ((1.18×10^{17} cm $^{-1}$) layers was also established. The performance of the n- CdS/ p- CH3NH3SnI3 perovskite solar cell was compared with the performance of the n- CdS/ p- $CH_3NH_3SnI_3$ perovskite solar cell with the application of the back surface layer and the results obtained were as follows before the addition of the (BSF) layer.

The results indicated that Jsc, Voc, FF and η were (25.4 mA/cm^2 , 0.81 V, 88, and 18.3 Upon introducing BSF layer, it was determined that Jsc, Voc, FF and eta were (34 mA/cm2,0.817V, 90 and 24.78) respectively as in Table.2.

Table.2 Comparative analysis of the working of the perovskite solar cell in the absence and presence of a BSF layer.

	Material	Thickness(µm)	Doping ($^{cm-3}$)	Jsc (mA/cm2)	Voc (V)	FF (%)	η (%)
Without InP BSF	CdS	0.03	$1.18\times 10^{17}cm^{-3}$	25.4	0.81	88	18.3
	$CH_3NH_3SnI_3$	5	$1.18\times 10^{17}cm^{-3}$				
With InP BSF	CdS	0.03	$1.18\times 10^{17}cm^{-3}$	34	0.81	90	24.78%
	$CH_3NH_3SnI_3$	5	$1.18\times 10^{17}cm^{-3}$				
	InP	5	$1.48\times 10^{17}cm^{-3}$				

3.3. Effect of temperature on electric properties of perovskit solar cell.

The operating temperature response to the electric properties of the proposed perovskite solar cell is investigated as shown in. Figure 10. with an operating temperature of 300K to 400K with p-type absorption layer thickness 5 µm (doping concentration: $1.18\times 10^{17}cm^{-3}$), n-type window layre thickness 0.03 µm (doping concentration: $1.18\times 10^{17}cm^{-3}$), and p-type BSF layer thickness 5 µm (doping concentration: $1.45\times 10^{17}cm^{-3}$) to gain improved stability of the perovskite solar cell. It is established that Voc declined drastically to 0.65 V at an increase in operating temperature whereas short circuit current is nearly constant with the increase in temperature. The conversion efficiency also reduced with increasing in temperature between 300k and 400k to 18.87%. The behavior is consistent with the earlier reported temperature dependent solar cell performance in the literature (Bouich et al., 2019; Heriche et al., 2017). Optimized design J-V curve was plotted by varying the Temperature of 300K to 400K by 10K at a time and the results were entered in Table 3.

Table 3. Perovskite Solar Cell Performance with Operating Temperature.

T (Kelvin)	Jsc (mA/cm2)	Voc (Volt)	%η
300	34.06	0.81	**24.68**
310	34.10	0.79	**24.10**
320	34.13	0.78	**23.52**

T (Kelvin)	Jsc (mA/cm2)	Voc (Volt)	%η
330	34.17	0.76	**22.94**
340	34.21	0.75	**22.36**
350	34.25	0.73	**21.78**
360	34.29	0.71	**21.20**
370	34.34	0.70	**20.61**
380	34.39	0.68	**20.04**
390	34.44	0.66	**19.45**
400	34.49	0.65	**18.87**

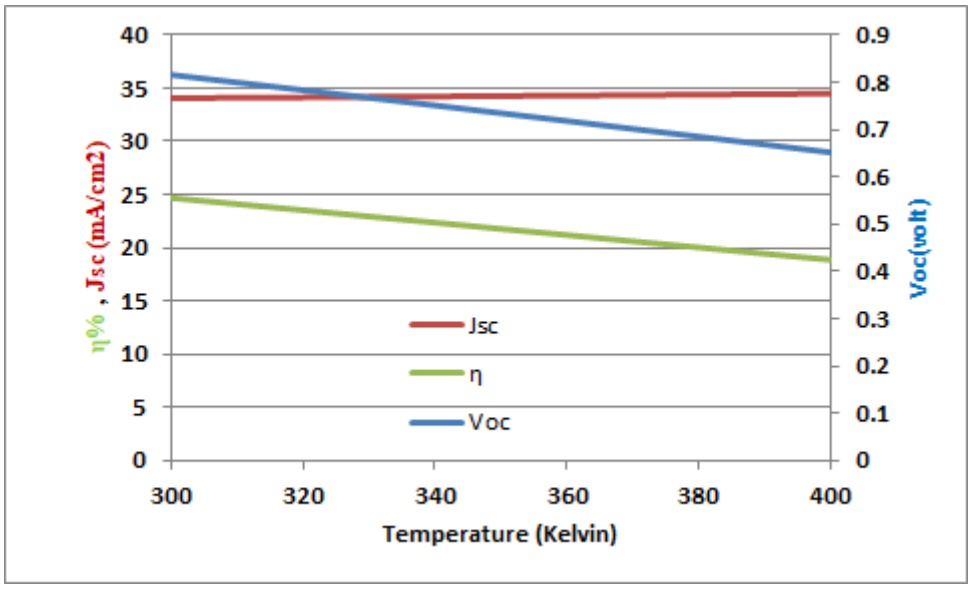

Figure 10. Variation of short circuit current , open circuit voltage and conversion efficiency with operating temperature (0.5-5)µm.

4. Conclusion

In this paper,perovskite solar cell layers of n -CdS / p - $CH_3NH_3SnI_3$ / p -InP were designed, and their performance was analyzed by PC1D simulation tool. Numerical simulation were performed to get insight performance of the proposed solar cell by incorporating back surface field layer and different thickness, doping concentration and operating temperature. The simulation outcomes show that it is possible to obtain great performance of photovoltaic by employing a solar cell with a back surface field layer. It yielded the Photovoltaic cell parameters namely V_{oc} of 0.81V, J_{sc} of 34 mA/cm^2, a FF of 90 percent and an efficiency of 24.78 percent at thickness 5.0 µm and doping concentration $1.18x10^{-17}$ cm^{-3} of the $CH_3NH_3SnI_3$ absorber layer. Last tested was the influence of temperature on the final cell were the temperature was varied between 300k and 400k. Optimal cell properties were observed at 300k temperature as indicated in table.3.

References

Ahmed, M. S., Ahmad, S. M., & Subhyaljader, M. (2020). Study the role of effective parameters in enhancement of the silicon solar cell performance using PC1D simulation. Journal of Ovonic Research, 16(2), 97–106.

Banerjee, S. (2015). International Journal of Engineering Research & Technology, 4.

Bouich, A., Hartiti, B., Ullah, S., Ullah, H., Touhami, M. E., Santos, D. M. F., & Mari, B. (2019). Optik, 183, 137.

Britt, J., & Ferekides, C. (1993). Thin film CdS/CdTe solar cell with 15.8% efficiency. Applied Physics Letters, 62(22), 2851.

Du, H.-J., Wang, W.-C., & Zhu, J.-Z. (2016). Device simulation of lead-free $CH_3NH_3SnI_3$ perovskite solar cells with high efficiency. Chinese Physics B, 25(10), 108802.

Duenow, J. N., Gessert, T. A., Wood, D. M., Barnes, T. M., Young, M., To, B., & Coutts, T. J. (2007). Transparent conducting zinc oxide thin films doped with aluminum and molybdenum. Journal of Vacuum Science & Technology A: Vacuum, Surfaces, and Films, 25(4), 955–960.

Green, M. A., Emery, K., Hishikawa, Y., Warta, W., & Dunlop, E. D. (2012). Solar cell efficiency tables (version 40). Progress in Photovoltaics: Research and Applications, 20(5), 606–614.

Green, M. A., Ho-Baillie, A., & Snaith, H. J. (2014). The emergence of perovskite solar cells. Nature Photonics, 8(7), 506–514.

Hamoodi, A. N., Abdulla, F. S., & Alwan, A. A. (2022). A comparison study among optimization methods for solar PV hybrid system. NTU Journal of Engineering and Technology, 1(4).

Heriche, H., Rouabah, Z., & Bouarissa, N. (2017). International Journal of Hydrogen Energy, 42, 9524.

Kapadnis, R. S., Bansode, S. B., Supekar, A. T., Bhujbal, P. K., Kale, S. S., Jadkar, S. R., & Pathan, H. M. (2020). Cadmium telluride/cadmium sulfide thin films solar cells: A review. ES Energy & Environment, 10, 3–12.

Lee, S. H., Lee, D. W., Shin, E. G., & Lee, S. H. (2016). Current Photovoltaic Research, 4(1), 12.

Li, M.-H., Yum, J.-H., Moon, S.-J., & Chen, P. (2016). Inorganic p-type semiconductors: Their applications and progress in dye-sensitized solar cells and perovskite solar cells. Energies, 9(5), 331.

López-Ernández, I., et al. (2024). Lead-free halide perovskite materials and optoelectronic devices: Progress and prospective. Advanced Functional Materials, 34(6).

Luque, A., & Hegedus, S. (2011). Handbook of photovoltaic science and engineering. Wiley.

Mandong, A., & Uzum, A. (2019). Analysis of silicon solar cell device parameters using PC1D. ResearchGate. https://www.researchgate.net/publication/336445702

Nahid, M. N., et al. (2024). Optimizing lead-free $CH_3NH_3SnI_3$ perovskite solar cells by using SCAPS-1D software. Chemistry of Inorganic Materials, 4, 100069.

Noel, N. K., et al. (2014). Lead-free organic–inorganic tin halide perovskites for photovoltaic applications. Energy & Environmental Science, 7(9), 3061–3068.

Ngoupo, A. T., Ouédraogo, S., & Ndjaka, J. M. (2019). Numerical analysis of interface properties effects in CdTe/CdS:O thin film solar cell by SCAPS-1D. Indian Journal of Physics, 93(7), 869–881.

Parajuli, D., Shah, D. K., KC, D., Kumar, S., & Park, M. (2022). Influence of doping concentration and thickness of regions on the performance of InGaN single junction-based solar cells: A simulation approach. Electrochemistry, 3, 407–415.

Pourdadash, M. H., Thangasamy, V., Lukose, J., Aghaei, M., & Shah, A. H. (2014). Numerical analysis on prospects of high efficiency CdS/CdTe thin film solar cell. In Proceedings of IEEE Symposium on Industrial Electronics & Applications (ISIEA) (pp. 86–91). IEEE.

Qin, P., et al. (2014). Inorganic hole conductor-based lead halide perovskite solar cells with 12.4% conversion efficiency. Nature Communications, 5(1).

Ram Sevak, S., Kumar, S. A., Anurag, G., Varun, R., & Kumar, J. M. (2023). Modeling and simulation of thin film InP/GaAs dual-junction solar cells. Iranian Journal of Chemistry and Chemical Engineering, 42(10).

Rassol, R. A., Hasan, R. F., & Ahmed, S. M. (2021). Numerical analysis of SnO_2/Zn_2SnO_4/n-CdS/p-CdTe solar cell using the SCAPS-1D simulation software. Iraqi Journal of Science, 62(2), 505–516.

Repins, I., Contreras, M. A., Egaas, B., et al. (2008). 19.9%-efficient ZnO/CdS/$CuInGaSe_2$ solar cell with 81.2% fill factor. Progress in Photovoltaics: Research and Applications, 16(3), 235–239.

Singh, R., Singh, P. K., Bhattacharya, B., & Rhee, H. W. (2019). Review of current progress in inorganic hole transport materials for perovskite solar cells. Applied Materials Today, 14, 75–200.

Song, T.-B., Yokoyama, T., Aramaki, S., & Kanatzidis, M. G. (2017). Performance enhancement of lead-free tin-based perovskite solar cells with reducing atmosphere-assisted dispersible additive. ACS Energy Letters, 2(4), 897–903.

Thirunavukkarasu, G. S., Seyedmahmoudian, M., Chandran, J., Stojcevski, A., Subramanian, M., Marnadu, R., Alfaify, S., & Shkir, M. (2021). Energies, 14, 4986.

Tuo, S., Kevin, K. B. M., Kamenan, K. A., Datte, J., & Yapi, A. S. (2024). SCAPS 1D simulation of a lead-free perovskite photovoltaic solar cell using hematite as electron transport layer. Modeling and Numerical Simulation of Material Science, 14, 97–106.